Nuclear Science and Techniques (2025) 36:125
https://doi.org/10.1007/s41365-025-01705-4

Study on photoluminescence and thermoluminescence of $Y_{2-x}Sm_xMgTiO_6$ phosphors

Hao Liu[1] · Lu-Yan Wang[1] · Zheng-Ye Xiong[1] · Jing-Yuan Guo[1]

Received: 20 March 2024 / Revised: 23 July 2024 / Accepted: 25 July 2024 / Published online: 10 May 2025

Abstract

Double perovskite matrix materials have recently attracted considerable interest due to their structural flexibility, ease of doping, and excellent thermal stability. While photoluminescence (PL) studies of rare-earth-doped double perovskites are common, research on their thermoluminescence (TL) properties is less extensive. This study synthesized a series of $Y_{2-x}Sm_xMgTiO_6$ ($0 \le x \le 0.1$) samples using a high-temperature solid-state method. X-ray diffraction (XRD) analysis confirmed a monoclinic crystal structure (space group $P2_1/n$), with Sm^{3+} ions substituting for Y^{3+} ions in Y_2MgTiO_6. The PL results indicated that the optimal doping concentration was $Y_{1.95}Sm_{0.05}MgTiO_6$, exhibiting emission peaks at 568, 605, 652, and 715 nm under 409 nm blue light excitation. The TL measurements for different doping concentrations showed that the $Y_{1.98}Sm_{0.02}MgTiO_6$ phosphors exhibited the strongest TL signals. The TL peaks observed at 530 and 610 K correspond to defects in the matrix and Sm^{3+} dopants, respectively. The $T_m - T_{stop}$ analysis revealed that the TL curve of $Y_{1.98}Sm_{0.02}MgTiO_6$ phosphors was a superposition of seven peaks. Computerized glow curve deconvolution (CGCD) was performed on the TL of the sample according to the results of three-dimensional thermoluminescence spectra (3D-TL) and $T_m - T_{stop}$, and the trap depths in the sample were estimated to range from 0.69 to 1.49 eV. Additionally, the lifetimes of each overlapping peak were calculated using the fitting parameters. Furthermore, the dose–response test showed that the saturation dose of the sample was high (9956 Gy). Therefore, this material can serve as a thermoluminescent dosimeter for high-dose measurements. The saturation dose for the lowest-temperature overlapping peak was 102 Gy, which correlated with its specific energy-level lifetime, whereas the other overlapping peaks also exhibited favorable linear relationships.

Keywords Y_2MgTiO_6 · Thermoluminescence · $T_m - T_{stop}$ · Computerized glow curve deconvolution · Dose–response

1 Introduction

Studies have shown that the optical and dosimetric properties of oxide matrix materials doped with rare-earth ions can be improved [1–5]. Double perovskites have attracted considerable attention among oxide matrix materials because of their excellent chemical structure and good stability [6]. $AA_1BB_1O_6$-type double perovskites can be obtained by partially substituting A or B sites of ABO_3-type simple perovskites with different A_1 or B_1 ions. The structure and luminescence properties of double perovskites, a new type of matrix material, have been extensively studied. For example, La_2MgTiO_6 [7], Gd_2ZnTiO_6 [8], La_2MTiO_6 (M=Co,Ni) [9] have good thermal stability and superior luminescence properties, which can be used as candidate materials in the field of lighting. However, their thermoluminescent properties have rarely been studied. Y_2MgTiO_6 matrix materials have become a research hotspot in recent years, owing to their physicochemical stability, easy preparation, and wide availability as raw materials [10].

Thermoluminescent materials contain a certain concentration of luminescent centers and traps. Under high-energy

This work was supported by the Zhanjiang Science and Technology Plan Project (No. 2022A05022), Science and Technology Development Special Project of Zhanjiang (No. 2023A21616) and Research Project of Guangdong Ocean University (No. 060302112102).

✉ Zheng-Ye Xiong
xiongzhengye@139.com

Jing-Yuan Guo
gjy3344@126.com

[1] School of Electronic and Information Engineering, Guangdong Ocean University, Zhanjiang 524088, China

radiation excitation, free electrons and holes are generated in the crystal, some captured by traps. When a crystal is heated, the captured electrons (or holes) are thermally excited to become quasi-free carriers, and thermoluminescence is produced when the quasi-free carriers recombine with the luminescent centers [11, 12]. Analysis of the thermoluminescence glow curve can be used to estimate the types and activation energies of the traps [13–16]. Most current studies use the computerized glow curve deconvolution (CGCD) method for analysis. If the internal information of the system is unknown, the method lacks physical meaning. If the luminescence characteristics of thermoluminescent materials are further elucidated, the results can be more accurate and reliable. Many thermoluminescent materials have good dose–response linearity, easy fabrication, and low cost [17–19], and can be used for ionizing radiation dose detection. For example, LiF:Mg,Cu,P [20], $Li_2B_4O_7$:Mn [21] can be used for personal dose detection; BeO [22], $CaSO_4$:Dy [23], CaF_2:Dy [24]can be used for environmental dose detection; Al_2O_3:C [25], MgB_4O_7:Dy [26] can be applied to medical dose detection. In addition to the standard thermoluminescence dosimeters, there are other materials that may be used for dose detection, such as $SrGd_2O_4$:Sm, $SrDy_2O_4$:Eu, $BaSi_2O_5$:Dy, (Sr,Ba)AlO_4:Eu/Dy, $CaWO_4$:Pr, $LaGa_4O(BO_3)_3$ and (Ba,Sr)TiO_3:Pr [27–32]. Generally, the sensitivity of thermoluminescence dosimeters is high; however, the linear upper limit of the dose–response is generally low (approximately 200 Gy). On special occasions (such as during irradiation preservation), it is often necessary to accurately measure the irradiation dose at the kGy level [33, 34]. Therefore, studying thermoluminescent materials with stable performance and a wide linear dose–response range can broaden the applications of thermoluminescence technology.

A Sm^{3+} single-doped Y_2MgTiO_6 phosphor was prepared using a high-temperature solid-state method, and its X-ray diffraction (XRD), photoluminescence (PL), and thermoluminescence (TL) were measured. The thermoluminescence mechanism of the sample exhibiting the highest TL yield, along with its potential for use as a thermoluminescent dosimeter and high-dose detection, was investigated using three-dimensional thermoluminescence spectroscopy(3D-TL), $T_m - T_{stop}$ analysis, CGCD method and dose–response.

2 Experiment

2.1 Sample preparation

$Y_{2-x}Sm_xMgTiO_6$ ($x = 0, 0.001, 0.002, 0.005, 0.01, 0.02, 0.05, 0.1$ and 0.2) phosphors were synthesized using a high-temperature solid-state method. Stoichiometric amounts of Y_2O_3 (99.99%), MgO (99.99%),TiO_2 (99.99%), Sm_2O_3 (99.99%) were weighed and placed in an agate mortar for 0.5 h until a homogenous mixture was achieved. This uniformly ground powder was placed in a corundum crucible in a muffle furnace and pre-sintered in the air at 800 °C for 3 h. Subsequently, the temperature was rapidly increased to 1300 °C at a faster heating rate (7 °C s^{-1}), and the samples were calcined at 1300 °C for 9 h. The resulting block-shaped sintered products were then crushed and ground again using an agate mortar to obtain the final phosphor powder.

2.2 Testing method

X-ray diffraction (XRD) patterns were recorded using a Rigaku Ultima IV X-ray diffractometer with a Cu-K_α radiation source, a scanning range of 10° to 80°, and a scanning rate of 5°/min. Photoluminescence (PL) spectra were measured using a HITACHI F-7000 fluorescence spectrometer with a Xe lamp excitation source and a spectral resolution of 0.2 nm. Thermoluminescence (TL) measurements were performed using a Risø TL/OSL-15-B/C thermoluminescence/optically stimulated luminescence measurement instrument equipped with a $^{90}Sr\beta$ radiation source (1.4 GBq activity, 0.1 Gy/s dose rate). The distance between $^{90}Sr\beta$ radiation source and the sample was 5 mm, the distance between the detector and the sample was 55 mm, and the heating rate was 5 K/s during measurement. The three-dimensional thermoluminescence spectroscopy of the samples was measured using an LTTL3DS thermoluminescence spectrometer (Guangzhou Ruidi Technology Co., Ltd.). The irradiation source was an X-ray tube, the working voltage of the X-ray tube was 50 kV, the current was 150 μA, the dose rate was about 0.1 Gy/s, the heating rate was 5 K/s during measurement, the heating range was 300–750 K, the spectral range was 300–1000 nm, and the spectral resolution was 1 nm.

3 Results and discussion

3.1 XRD analysis

The XRD patterns of $Y_{2-x}Sm_xMgTiO_6$ ($x = 0, 0.005, 0.01, 0.02, 0.05$ and 0.1) series samples are shown in Fig. 1. No information on Y_2MgTiO_6 is available in the inorganic crystal information database. Shannon [35] used the Rietveld method to analyze data, and the results proved that Dy_2MgTiO_6 and Y_2MgTiO_6 have very similar structures. Therefore, the standard Dy_2MgTiO_6 (ICDD 04-021-1637) card was used as a reference. As shown in the figure, the number and positions of the diffraction peaks for all samples are consistent

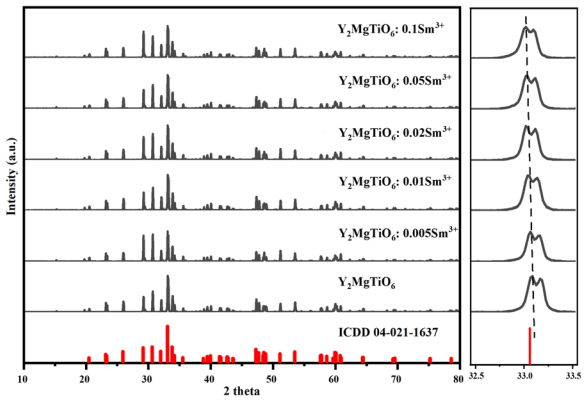

Fig. 1 XRD spectra of $Y_{2-x}Sm_xMgTiO_6$ ($x = 0, 0.005, 0.01, 0.02, 0.05$ and 0.1) samples

with the standard card. The diffraction angle at 33°, corresponding to the characteristic site of Y^{3+} shifts to a small angle [36, 37]. According to Bragg's equation [38, 39], this decrease in diffraction angle indicates an increase in lattice spacing. Given the ionic radii of $rY^{3+} = 0.1019$ nm, $rMg^{2+} = 0.0720$ nm, $rTi^{4+} = 0.0605$ nm [40], and the ionic radius of Sm^{3+} is $rSm^{3+} = 0.1132$ nm. The shift in the diffraction angle of the characteristic site of Y^{3+} to a small angle confirms the successful substitution of Y^{3+} by the larger Sm^{3+} ions within the lattice. This substitution does not alter the overall lattice structure or charge configuration, and the samples retain the monoclinic $P2_1/n$ [37].

Figure 2 shows the morphology and lattice fringes of Y_2MgTiO_6 matrix and Y_2MgTiO_6:Sm. The figure reveals that the phosphor particles have irregular morphologies, with sizes ranging from approximately 400 nm to 2 µm. After Sm doping, the lattice fringes become denser, indicating decreased crystal plane spacing. This observation further supports the successful incorporation of the larger Sm ions into the matrix lattice. Combined with the XRD results, this confirms the successful synthesis of the phosphor under the described experimental conditions.

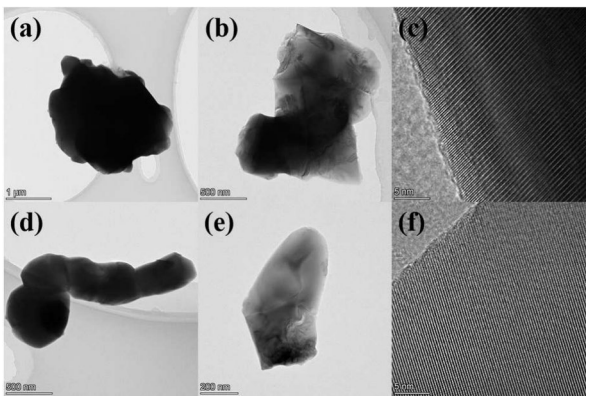

Fig. 2 TEM of $Y_{2-x}Sm_xMgTiO_6$

3.2 Photoluminescence analysis

Figure 3 shows the PL of $Y_{2-x}Sm_xMgTiO_6$ ($x = 0.001, 0.002, 0.005, 0.01, 0.02, 0.05$ and 0.1) series phosphors. With a monitoring wavelength of 605 nm, the excitation spectrum spanned from 340 to 500 nm. The strongest absorption peak is at 409 nm, which belongs to the characteristic transition of $Sm^{3+}{}^6H_{5/2} \rightarrow {}^6P_{3/2}$. The absorption peaks at 349 nm, 366 nm, 379 nm, 422 nm, 443 nm, and 474 nm correspond to the characteristic transitions of $Sm^{3+}\,{}^6H_{5/2} \rightarrow {}^4H_{9/2}, {}^4D_{3/2}, {}^6P_{7/2}, {}^6P_{5/2}, {}^4F_{5/2}, {}^4I_{13/2}$, respectively [41]. When excited by 409 nm purple light, four prominent emission peaks are observed at 568 nm, 605 nm, 652 nm and 715 nm, corresponding to the characteristic transitions of $Sm^{3+}\,{}^4G_{5/2} \rightarrow {}^6H_{5/2}, {}^6H_{7/2}, {}^6H_{9/2}, {}^6H_{11/2}$, respectively [42, 43]. With increasing Sm^{3+} doping concentration, the positions and shapes of the emission peaks remained unchanged, while the intensity initially increased and subsequently decreased. The optimal doping concentration was found to be $x = 0.05$, where the photoluminescence emission intensity reached a maximum. Further increases in the Sm^{3+} doping concentration significantly decreased emission intensity, indicating concentration quenching.

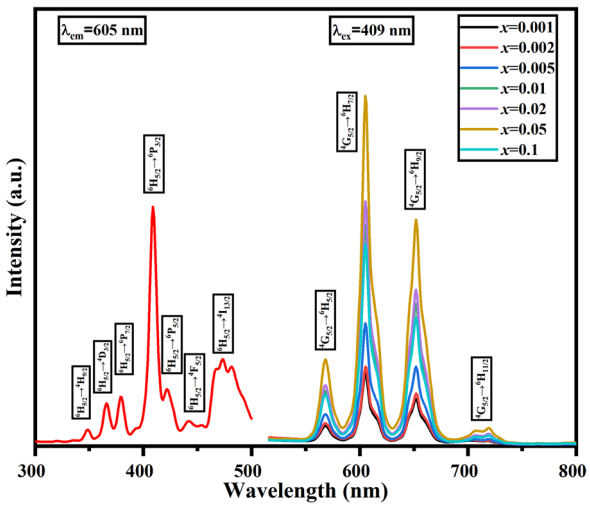

Fig. 3 (Color online) Photoluminescence spectra of $Y_{2-x}Sm_xMgTiO_6$ ($x = 0.001, 0.002, 0.005, 0.01, 0.02, 0.05$ and 0.1) samples

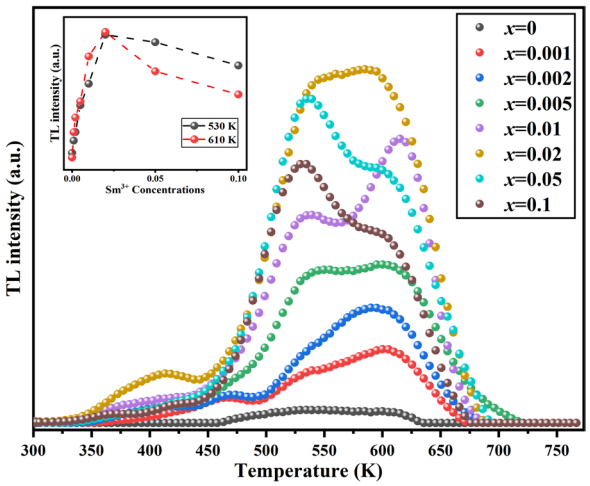

Fig. 4 (Color online) The thermoluminescence spectra of $Y_{2-x}Sm_xMgTiO_6$ ($x = 0, 0.001, 0.002, 0.005, 0.01, 0.02, 0.05$ and 0.1) samples by irradiate with $^{90}Sr\beta$ radiation source for 100 Gy. The variation trend of thermoluminescence intensity with Sm^{3+} doping concentration at 530 K and 610 K is illustrated

3.3 Doping concentration optimization

The thermoluminescence response was optimized by varying the doping concentration of Sm^{3+} to determine the phosphor with the best TL yield. Samples with different doping concentrations (30 mg each) underwent TL testing using the following procedure: (1) preheating to 773 K for 10 s; (2) cooling to room temperature; (3) irradiation with a $^{90}Sr\beta$ radiation source at a dose of 100 Gy; (4) TL measurement at a heating rate of 5 K/s. The measurement results are presented in Fig. 4. As can be seen from the figure, with an increase in the Sm^{3+} doping concentration, the integrated TL intensity also increased, reaching a maximum at $x = 0.02$, which was then selected for subsequent experiments. Further increases in Sm^{3+} concentration led to concentration quenching and decreased integrated thermoluminescence intensity. It can be seen from the figure that the Y_2MgTiO_6 matrix has a weak thermoluminescence peak, and the thermoluminescence range is between 460 K and 630 K. After introducing Sm^{3+}, the thermoluminescence peak of the phosphor extended to the high-temperature zone. There was evident thermoluminescence at 675 K. In addition, the shape of the thermoluminescence curve changes with the Sm^{3+} doping concentration. As shown in the inset of Fig. 3, when the Sm^{3+} doping concentration was $x < 0.02$, the thermoluminescence peak around 610 K was more intense than the peak at approximately 530 K. Conversely, for Sm^{3+} doping concentrations $x > 0.02$, the thermoluminescence peak at approximately 530 K exhibited a higher intensity than the peak at approximately 610 K. At a Sm^{3+} doping concentration of $x = 0.02$, a balanced state is observed between the intensities of the two prominent TL peaks. However, when concentration quenching occurs at higher doping levels, the peak intensity at approximately 610 K decreases more rapidly than at approximately 530 K.

To elucidate the underlying mechanisms responsible for the observed thermoluminescence behavior of $Y_{2-x}Sm_xMgTiO_6$ series phosphors, three-dimensional thermoluminescence (3D-TL) spectra were acquired for four representative samples irradiated with 100 Gy of X-rays, as shown in Fig. 5. Figure 5a shows that the thermoluminescence range of Y_2MgTiO_6 matrix is between 480 K and 640 K, with peak temperatures at approximately 530 K and 600 K, consistent with the TL glow curve shown in Fig. 4. The characteristic emission band for Y_2MgTiO_6 matrix is centered at 698 nm. Figure 5b presents the three-dimensional thermoluminescence spectrum of the sample doped with $0.01Sm^{3+}$. The introduction of Sm^{3+} enhances the thermoluminescence intensity of Y_2MgTiO_6 matrix without altering the peak temperature or emission band position of the matrix thermoluminescence. A new thermoluminescence peak appears around 610 K, with emission bands around 570 nm, 600 nm, and 650 nm, consistent with the characteristic, and the emission band is around 570 nm, 600 nm, 650 nm, which is consistent with the characteristic Sm^{3+} emissions obtained in PL. This confirms that this TL peak originates from Sm^{3+}. The Sm^{3+} -related TL intensity is significantly higher than that of the matrix, meaning that the peak intensity around 610 K is larger than that of 530 K, consistent with the curve in Fig. 4. The three-dimensional thermoluminescence spectrum for the Sm^{3+} doping concentration of $x = 0.02$ is shown in Fig. 5c. As the Sm^{3+} doping concentration increases, the thermoluminescence intensity intensity of

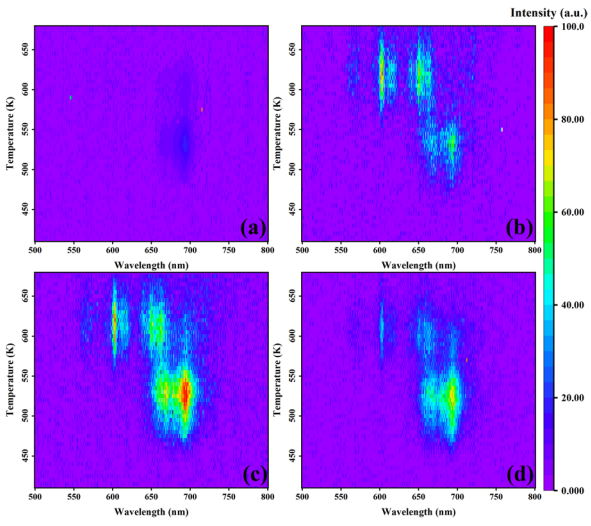

Fig. 5 (Color online) The thermoluminescence spectra of Y_2MgTiO_6 **a**,$Y_{1.99}Sm_{0.01}MgTiO_6$ **b**,$Y_{1.98}Sm_{0.02}MgTiO_6$ **c** and $Y_{1.9}Sm_{0.1}MgTiO_6$ **d** samples by irradiating with X-Ray source for 100 Gy

both Sm^{3+} and the matrix is enhanced. At this concentration $x = 0.02$, the thermoluminescence peak intensity of Sm^{3+} (610 K) is comparable to that of the matrix (530 K), achieving a balanced state. Further increases in Sm^{3+} concentration result in a significant decrease in the Sm^{3+} -related thermoluminescence intensity, while the matrix thermoluminescence intensity also decreases, but to a lesser extent. This indicates that the Sm^{3+} thermoluminescence emission is strongly affected by concentration quenching, while the matrix TL is less affected. This explains why the 530 K thermoluminescence peak becomes more intense than the 610 K peak at higher Sm^{3+} concentrations Th

To determine the energy dependence of the thermoluminescence under X-ray and β -particles irradiation, the thermoluminescence spectra of four samples under X-ray irradiation were measured using the Risø instrument and compared with the thermoluminescence spectra obtained under β -particles irradiation. The results are presented in Fig. 6. The thermoluminescence spectra under both X-ray and β -particle irradiation are broadly similar, with only minor differences observed in the low-temperature region.

3.4 $T_m - T_{stop}$ method

To confirm the number of overlapping peaks and their respective peak temperatures in the thermoluminescence (TL) spectrum of $Y_{1.98}Sm_{0.02}MgTiO_6$, fitting was performed using the CGCD method, and the thermal luminescence mechanism and kinetic parameters of the sample were further explored. Peak-separation experiments were performed using $T_m - T_{stop}$. The test steps for the $T_m - T_{stop}$ method are as follows.

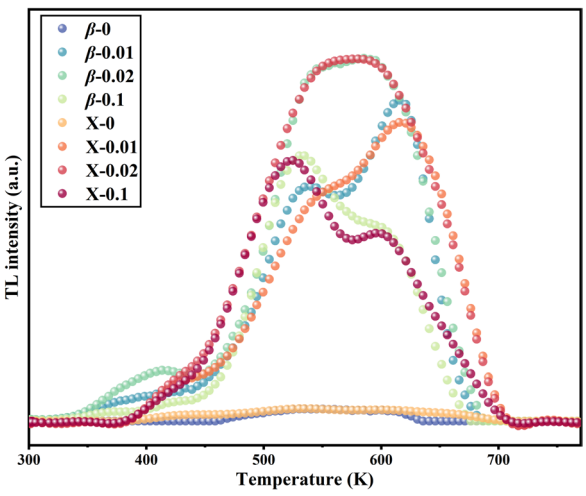

Fig. 6 (Color online) Thermoluminescence spectra of $Y_{2-x}Sm_xMgTiO_6$ phosphors irradiated by X-ray and β-particles at 100 Gy

1. The samples were preheated to 773 K and held for 10 s.
2. The samples were then cooled to room temperature.
3. The samples were irradiated using a $^{90}Sr\beta$ radiation source at a dose of 100 Gy.
4. The samples were then heated to a sufficiently high temperature (T_{stop}), to clear the TL signal prior to the T_{stop} temperature value.
5. The samples were rapidly cooled to room temperature.
6. The samples were then reheated at the same heating rate (5 K/s), recording the remaining TL curve and noting the position of the first maximum, T_m, on the TL curve was recorded. This process was repeated with successively lower T_{stop} values (decreasing by approximately 3 K each time). Figure 7 shows the relationship between T_m and T_{stop}, revealing seven plateaus, each corresponding to a distinct TL peak. The T_m values for these overlapping peaks were determined to be 384, 419, 449, 532, 581, 610, and 640 K. Within the temperature range up to 449 K, the peak temperatures of the three lowest-temperature peaks varied with T_{stop}, indicating a significant trap recapture process characteristic of second-order kinetics. Above 532 K, the peak temperatures of the remaining four peaks remained relatively constant with changing T_{stop}, suggesting that trap recapture is negligible and consistent with first-order kinetics.

3.5 Computerized glow curve deconvolution (CGCD)

Computerized glow curve deconvolution (CGCD) is a widely used technique for analyzing complex TL mechanisms. It allows for determining the position, shape, and kinetic parameters of overlapping peaks within a TL glow curve[44]. In this study, CGCD, in conjunction with the results obtained from three-dimensional thermoluminescence spectroscopy and the $T_m - T_{stop}$ method, was used

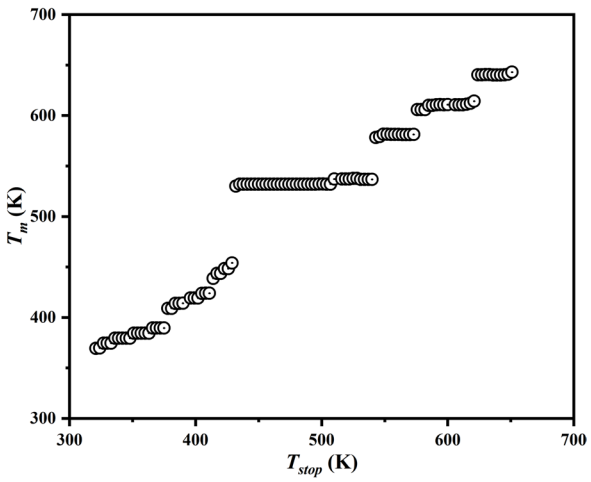

Fig. 7 $T_m - T_{stop}$ diagram of $Y_{1.98}Sm_{0.02}MgTiO_6$ sample

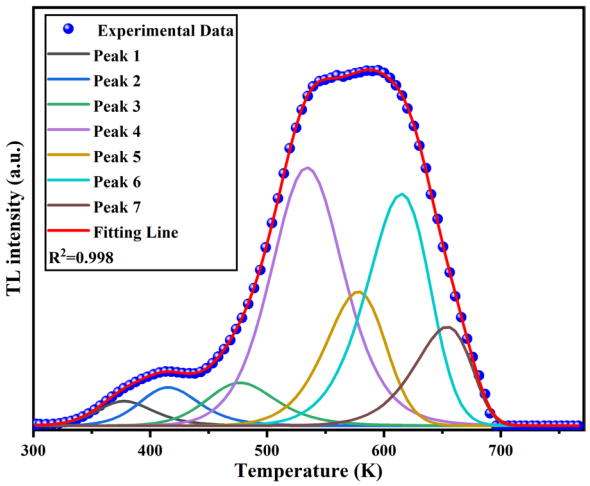

Fig. 8 (Color online) The TL curve fitting of $Y_{1.98}Sm_{0.02}MgTiO_6$ phosphor by irradiate with $^{90}Sr\beta$ radiation source for 100 Gy was carried out by CGCD method

Table 1 The kinetic parameters of $Y_{1.98}Sm_{0.02}MgTiO_6$ phosphor were analyzed by CGCD method

Peaks	E (eV)	T_m (K)	b	s (s^{-1})	τ (s)
1	0.69	378	2.0	3.95×10^{8}	9.8×10^{2}
2	0.81	415	2.0	1.52×10^{9}	2.6×10^{4}
3	0.91	477	2.0	9.52×10^{8}	2.0×10^{6}
4	1.03	534	1.6	9.96×10^{8}	2.0×10^{8}
5	1.22	578	1.2	9.29×10^{9}	3.3×10^{10}
6	1.29	615	1.2	7.04×10^{9}	6.5×10^{11}
7	1.49	654	1.0	5.93×10^{10}	1.8×10^{14}

to fit the TL glow curve of the $Y_{1.98}Sm_{0.02}MgTiO_6$ sample irradiated with 100 Gy from a $^{90}Sr\beta$ radiation source. Each overlapping peak can be described by Eq. 1 [45]:

$$I(t) = sn_0 \exp\left(-\frac{E}{kT}\right)\cdot\left[1+\frac{s(b-1)}{\beta}\cdot\int_{T_0}^{T}\exp\left(-\frac{E}{kT'}\right)dT'\right]^{-\frac{b}{b-1}}. \quad (1)$$

In Eq. 1: n_0 represents the initial number of captured electrons in the trap level; E is the activation energy of the captured electrons, in eV; s is the frequency factor, in Hz; k is the Boltzmann constant, which is 0.862×10^{-4} eV/K; β is the heating rate of the sample, in K/s, which is 5 K/s in this experiment; T is the absolute temperature (in units of K); b is the kinetic order. The CGCD fitting results are shown in Fig. 8. The fitting curve shows good agreement with the experimental data points, and the fitted parameters are presented in Table 1. These kinetic parameters were used to calculate the energy-level lifetime for each overlapping peak, which is a crucial parameter for estimating the saturation dose of each peak and is of significant importance for subsequent dose–response studies. The energy-level lifetimes for different overlapping peaks can be determined using Eq. 2 [46]:

$$\tau = s^{-1}\cdot e^{\left(\frac{E}{kT}\right)}. \quad (2)$$

In Eq. 2: τ represents the energy-level lifetime of the overlapping peak; s is the frequency factor for the overlapping peak; E denotes the trap depth of the overlapping peak; k is the Boltzmann constant; T stands for the ambient temperature (typically 300 K). After performing the calculations, the results are summarized in Table 1. The low-temperature peak at 378 K exhibits a relatively short lifetime of only 980 s, while deeper traps have longer lifetimes, as electrons trapped at shallower levels are more easily released. Figure 8 shows the results of CGCD fitting. The peak temperatures of the seven overlapping peaks are 378 K, 415 K, 477 K, 534 K, 578 K, 615 K, and 654 K, corresponding to trap depths ranging from 0.69 to 1.49 eV. The kinetic order b is 2.0 for the 378 K, 415 K, and 477 K peaks, 1.6 for the 534 K peaks, and approximately 1.0−1.2 for the 578 K, 615 K and 654 K peaks, consistent with the results obtained using the $T_m - T_{stop}$ method. Furthermore, the fitted peak temperatures for the overlapping peaks at 477, 534, 578, 615, and 654 K closely match those in Fig. 5c. Specifically, the three overlapping peaks at 477 K, 534 K, and 578 K are attributed to the Y_2MgTiO_6 matrix, while the overlapping peaks at 615 K and 654 K are associated with Sm^{3+}. The absence of the 378 K and 415 K peaks in Fig. 5c is likely due to experimental differences arising from the different excitation sources. These results demonstrate the scientific basis and reliability of the peak positions and kinetic parameters obtained through CGCD fitting based on investigating the system's internal mechanisms.

3.6 Dose–response

The TL dose–response test of $Y_{1.98}Sm_{0.02}MgTiO_6$ phosphor was investigated using the following procedure: (1) preheating the sample to 773 K for 10 s; (2) cooling to room temperature; (3) irradiating with ^{90}Sr radiation source at a dose of 2 Gy; and (4) measuring the TL emission (heating rate: 5 K/s). These steps were repeated, varying the irradiation dose to 5 Gy, 10 Gy, 20 Gy, 50 Gy, 60 Gy, 70 Gy, 80 Gy, 90 Gy, 100 Gy, 110 Gy, 120 Gy, 150 Gy, 200 Gy, 300 Gy, 400 Gy, 500 Gy, 700 Gy, 800 Gy, 900 Gy, 1000 Gy, 2000 Gy, 5000 Gy, 10,000 Gy, 20,000 Gy and 25,000 Gy. The resulting TK grow curves were recorded and are shown in Fig. 9. It can be seen that as the irradiation dose increased, the shape of the TL curve of the sample exhibited apparent changes. When the irradiation dose is less than 90 Gy, the peak value around 530 K is stronger, and the irradiation dose is more than 90 Gy, the peak

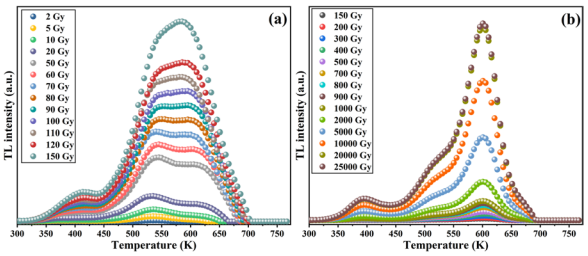

Fig. 9 (Color online) The thermoluminescence curves of $Y_{1.98}Sm_{0.02}MgTiO_6$ samples by irradiate with $^{90}Sr\beta$ radiation source for different doses

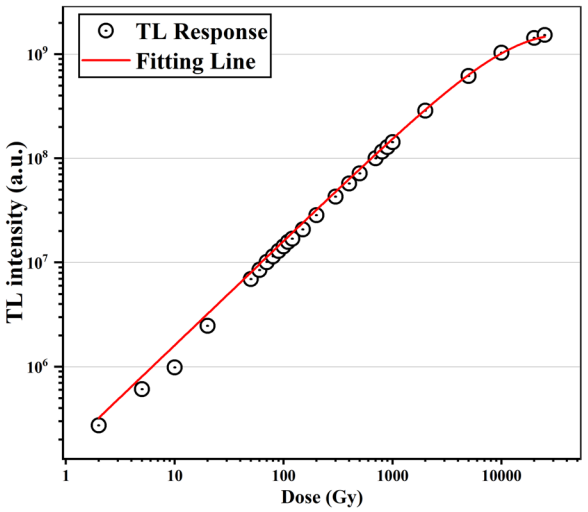

Fig. 10 Dose–response curve of $Y_{1.98}Sm_{0.02}MgTiO_6$ sample

value around 610 K is stronger, which indicates that the characteristic thermoluminescence of Sm^{3+} in $Y_{1.98}Sm_{0.02}MgTiO_6$ exhibits significantly higher sensitivity to radiation dose than the Y_2MgTiO_6 matrix.

Figure 10 shows the change in integrated TL intensity with increasing dose. Each data point in the figure represents the area under the TL glow curve. The dose–response appears to reach saturation and can be fitted using Eq. 3 [47]:

$$I(D) = A \cdot \left[1 - \exp\left(-\frac{D}{D_0}\right)\right]. \quad (3)$$

In Eq. 3: I represents the thermoluminescence integral intensity; A denotes the number of thermoluminescent sensitive units in the measured sample; D stands for the radiation dose; D_0 corresponds to the saturation dose. After fitting, it was found that the saturation dose of the sample was 9956 Gy. Compared with commonly used thermoluminescence dosimeters (e.g., LiF:(Mg,Cu,P),BeO,Al_2O_3:C), this material has a higher saturation dose, and the dose–response can still maintain good linearity at 1 kGy. Due to the easier release of trapped electrons at low temperatures, the decay times for the trapped electrons at 378 K and 415 K are relatively short (0.01 days and 0.3 days, respectively). However, the decay times for trapped electrons at 477 K and above are significantly longer (more than 23 days), indicating better signal stability. Therefore, this material's high saturation dose and long decay time suit high-dose radiation dosimetry applications, such as fruit irradiation preservation.

While it is possible to fit the dose–response of a TL curve with multiple overlapping peaks using the total integrated TL intensity at various irradiation doses, the significant differences in energy-level lifetimes among these peaks can introduce theoretical deviations. However, these deviations may be negligible within specific dose ranges. To investigate the dose–response characteristics of each individual overlapping peak in the $Y_{1.98}Sm_{0.02}MgTiO_6$ phosphor system, the CGCD method was employed to fit TL curves at various irradiation doses. The results are shown in Fig. 11. In Fig. 11, it can be observed that the peak temperatures T_m of Peaks 1, 2, and 3 shift toward lower temperatures as the irradiation dose increases, consistent with second-order kinetic behavior. Peaks 4, 5, 6, and 7, on the other hand, exhibit no significant change in T_m with increasing irradiation dose, aligning with first-order kinetic behavior and the results are consistent with those of $T_m - T_{stop}$ method.

With increasing irradiation dose, the thermoluminescence intensity of peak 1 plateaus beyond 200 Gy. The thermoluminescence integral intensity of each overlapping peak under different irradiation doses was determined to explore the dose–response curves of the different overlapping peaks, as shown in Fig. 11. The results are presented in Fig. 12. The other overlapping peaks, except for Peak 1, exhibit good linear dose–response relationships. Peaks 6 and 7 show similar slopes, as do Peaks 3, 4, and 5, suggesting that Peaks 6 and 7 originate from Sm^{3+}, while Peaks 3, 4, and 5 are associated with the matrix. The slope of peak 6 is significantly larger than that of peak 4, indicating that the characteristic thermoluminescence of Sm^{3+} is much more sensitive to the irradiation dose than the matrix. The dose–response of Peak 1 appears to reach saturation. After fitting this response using Eq. 3, the saturation dose for Peak 1 was determined to be 102.5 ± 3.2 Gy. Considering that the dose rate of the $^{90}Sr\beta$ radioactive source is 0.1 Gy/s, and the energy-level lifetime of Peak 1 is 980 s, it is estimated that Peak 1 reaches saturation at an irradiation dose of approximately 98 Gy, which agrees well with the experimental dose–response measurements. To increase the saturation dose of Peak 1, a higher dose-rate radiation source could be used. For precise measurements below 1 kGy, it would be suitable to eliminate Peak 1 and integrate the TL signal above 378 K. For measurements above 1 kGy, eliminating Peaks 1 and 2 (with a saturation dose of approximately 2.6 kGy) and integrating the TL signal above 415 K would be more appropriate.

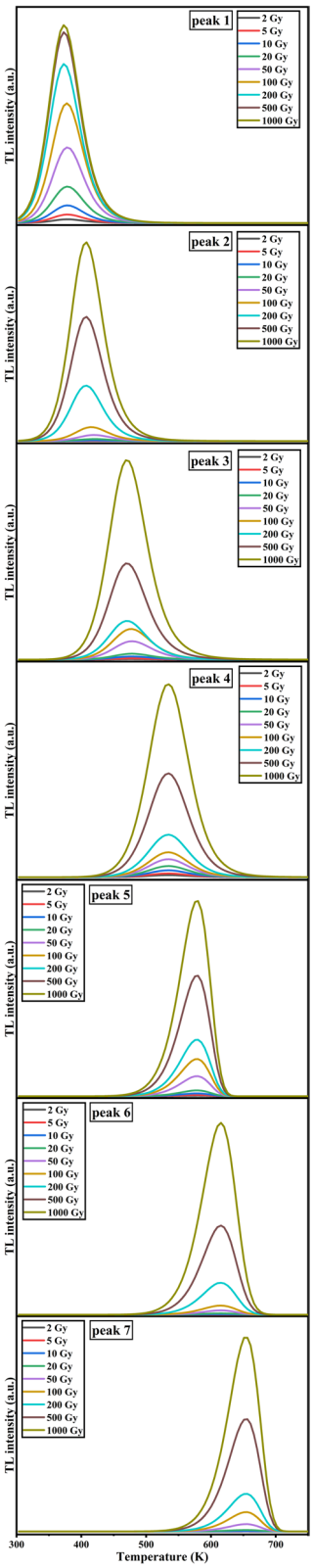

Fig. 11 (Color online) Overlapping peak curves at different irradiation doses

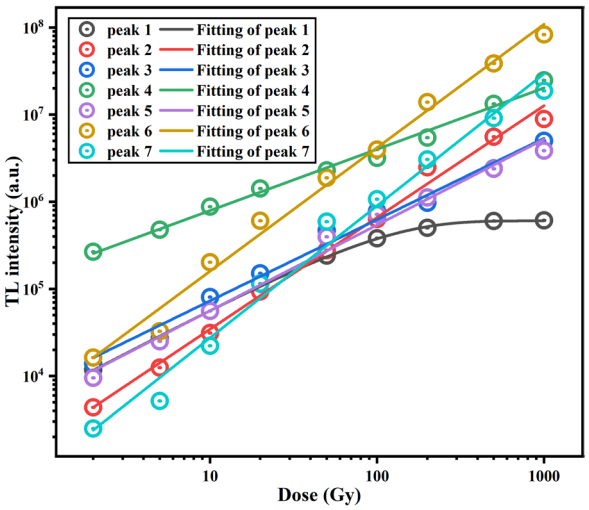

Fig. 12 (Color online) Dose response curves of different overlapping peak

3.7 Repeatability test

To verify the repeatability of the thermoluminescence (TL) signal, the TL curves of the $Y_{1.98}Sm_{0.02}MgTiO_6$ phosphor was subjected to repeated measurements under 100 Gy irradiation. Figure 13 shows the results of 12 measurements, where the total integral of the TL curve from each measurement was selected as the outcome and normalized. The experimental results indicated a relative standard error of approximately 0.06% for the measured TL signal, indicating minimal influence of radiation and temperature on the TL measurements.

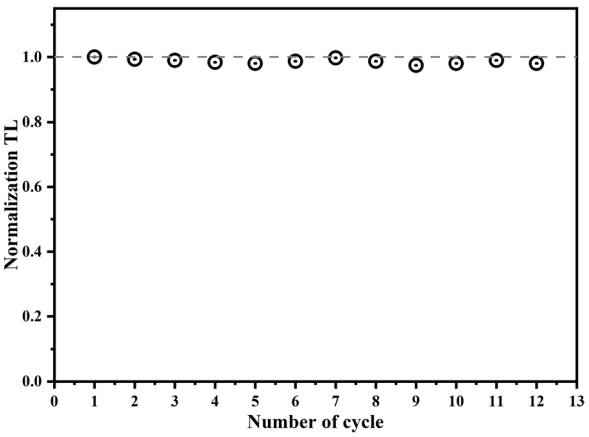

Fig. 13 Repetitive experiment of thermoluminescence

4 Conclusion

$Y_{2-x}Sm_xMgTiO_6$ $(0 \le x \le 0.2)$ series phosphors were synthesized using a high-temperature solid-state method. XRD confirmed the successful incorporation of Sm^{3+} into the Y^{3+} lattice sites. PL analysis revealed four emission peaks at 568, 605, 652, and 715 nm under 409 nm excitation. By analyzing the TL curve of the sample, it was found that the TL of $Y_{1.98}Sm_{0.02}MgTiO_6$ sample was the strongest, and three-dimensional thermoluminescence spectrum showed that the thermoluminescence around 530 K was attributed to Y_2MgTiO_6 matrix, and the thermoluminescence around 610 K was due to Sm^{3+} defects, which also proved that the matrix was less affected by concentration quenching than Sm^{3+}. $T_m - T_{stop}$ indicates that the thermoluminescence (TL) spectrum of this phosphor is a superposition of seven peaks. The T_m values for each overlapping peak were 384, 419, 449, 532, 581, 610, and 640 K. Additionally, the kinetic order of each peak was roughly estimated. Utilizing information from the three-dimensional thermoluminescence spectrum and the $T_m - T_{stop}$ method, the TL curve of the sample was fitted using the CGCD method, yielding reliable results. The trap parameters corresponding to the seven overlapping peaks are as follows: 0.69, 0.81, 0.91, 1.03, 1.22, 1.29, and 1.49 eV, with energy-level lifetimes of $9.8 \times 10^2, 2.6 \times 10^4, 2.0 \times 10^6, 2.0 \times 10^8, 3.3 \times 10^{10}, 6.5 \times 10^{11}, 1.8 \times 10^{14}$, respectively. The saturation dose of the $Y_{1.98}Sm_{0.02}MgTiO_6$ sample was 9956 Gy. Due to its good thermal stability and low production cost, this phosphor shows promise for high-dose radiation thermoluminescence dosimetry. Dose–response curves for each overlapping peak were generated for accurate dose monitoring. Within the 1 kGy range, Peak 1 saturated at 102 Gy, while the other peaks exhibited linear behavior. For precise dose measurements below 1 kGy, TL integration above 378 K is recommended; for doses above 1 kGy, integration above 415 K is preferable.

Author contributions All authors contributed to the study conception and design. Material preparation, data collection and analysis were performed by Hao Liu, Lu-Yan Wang, Zheng-Ye Xiong and Jing-Yuan Guo. The first draft of the manuscript was written by Hao Liu and all authors commented on previous versions of the manuscript. All authors read and approved the final manuscript.

Data availability The data that support the findings of this study are openly available in Science Data Bank at https://cstr.cn/31253.11.sciencedb.j00186.00616 and https://doi.org/10.57760/sciencedb.j00186.00616.

Declarations

Conflict of interest The authors declare that they have no Conflict of interest.

References

1. Y. Wang, H. Chen, F. Chen et al., Radiation dose detection using a high-power portable optically stimulated luminescence real-time reading system. Nucl. Sci. Tech. **29**(10), 63–71 (2018). https://doi.org/10.1007/s41365-018-0484-z
2. Z.W. Lv, G.X. Wei, H.Q. Wang et al., New flexible $CsPbBr_3$-based scintillator for X-ray tomography. Nucl. Sci. Tech. **33**(08), 36–46 (2022). https://doi.org/10.1007/s41365-022-01085-z
3. Y. Chuan, L.D.G. Xu, P.C. Zhang, Preparation and characterization of Bi_2O_3/XNBR flexible films for attenuating gamma rays. Nucl. Sci. Tech. **29**(07), 28–39 (2018). https://doi.org/10.1007/s41365-018-0436-7
4. S.L. Jin, R.F. Li, H. Huang, Compact ultrabroadband light-emitting diodes based on lanthanide-doped lead-free double perovskites. Light Sci. Appl. **11**, 52 (2022). https://doi.org/10.1038/s41377-022-00739-2
5. X.B. Li, Q. Liu, W.T. Huang, Structural and luminescent properties of Eu^{3+}-doped double perovskite $BaLaMgNbO_6$ phosphor. Ceram. Int. **44**(2), 1909–1915 (2018). https://doi.org/10.1016/j.ceramint.2017.10.130
6. C.Z. Guan, J. Zhou, H.L. Bao et al., Study of the relationship between the local geometricstructure and the stability of $La_{0.6}Sr_{0.4}MnO_{3-\delta}$ and $La_{0.6}$ $Sr_{0.4}$ $FeO_{3-\delta}$ electrodes. Nucl. Sci. Tech. **30**, 21 (2019). https://doi.org/10.1007/s41365-019-0550-1
7. Z.M. Chen, Z.Y. Wang, W.D. Kang, Preparation and luminescent properties of double perovskite-type La_{2-x-y} Y_x $MgTiO_6$: y Eu^{3+} red fluorescent materials. J. Lumin. **243**, 118656 (2022). https://doi.org/10.1016/j.jlumin.2021.118656
8. T. Zheng, L.H. Luo, P. Du, Highly-efficient double perovskite Mn^{4+}-activated Gd_2ZnTiO_6 phosphors: a bifunctional optical sensing platform for luminescence thermometry and manometry. Chem. Eng. J. **446**, 136839 (2022). https://doi.org/10.1016/j.cej.2022.136839
9. D.J. Hou, S.M. Zheng, Z.S. Lin et al., A Mn^{4+} activated $(Gd, La)_2(Zn, Mg)TiO_6$ deep-red emission phosphor: the luminescence properties and potential application for full-spectrum pc-LEDs. J. Lumin. **247**, 118895 (2022). https://doi.org/10.1016/j.jlumin.2022.118895
10. J.Q. Li, J.S. Liao, H.R. Wen, Multiwavelength near infrared downshift and downconversion emission of Tm^{3+} in double perovskite Y_2MgTiO_6:Mn^{4+}/Tm^{3+} phosphors via resonance energy transfer. J. Lumin. **213**, 356–363 (2019). https://doi.org/10.1016/j.jlumin.2019.05.038
11. J. Xu, S. Tanabe, Persistent luminescence instead of phosphorescence: history, mechanism, and perspective. J. Lumin. **205**, 581–620 (2019). https://doi.org/10.1016/j.jlumin.2018.09.047
12. H.H. Xiao, L.L. Liu, W.Y. Li et al., TLD calibration and absorbed dose measurement in a radiation-induced liver injury model under a linear accelerator. Nucl. Sci. Tech. **34**, 53 (2023). https://doi.org/10.1007/s41365-023-01211-5
13. X.M. Jin, Y. Liu, C.L. Su et al., Ionizing and non-ionizing Kerma factors in silicon for China spallation neutron source neutron spectrum. Nucl. Sci. Tech. **30**, 143 (2019). https://doi.org/10.1007/s41365-019-0664-5
14. Y.L. Liu, Q.X. Zhang, J. Zhang et al., Quantitative energy-dispersive X-ray fluorescence analysis for unknown samples using full-spectrum least-squares regression. Nucl. Sci. Tech. **30**, 52 (2019). https://doi.org/10.1007/s41365-019-0564-8
15. Y.H. Wang, Q. Li, L. Chen et al., Simulation study of the dose and energy responses of FNTD personal neutron dosimetry. Nucl. Sci. Tech. **30**, 32 (2019). https://doi.org/10.1007/s41365-019-0546-x
16. H. Yang, X.Y. Zhang, W.G. Gu et al., A novel method for gamma spectrum analysis of low-level and intermediate-level

radioactive waste. Nucl. Sci. Tech. **34**, 87 (2023). https://doi.org/10.1007/s41365-023-01236-w
17. K.N. Li, X.P. Zhang, Q. Gui et al., Characterization of the new scintillator Cs_2LiYCl_6:Ce^{3+}. Nucl. Sci. Tech. **29**, 11 (2018). https://doi.org/10.1007/s41365-017-0342-4
18. W. Tang, C.D. Zuo, Y.K. Li, Exploiting intervalence charge-transfer engineering to finely control (Ba, Sr)TiO_3:Pr^{3+} luminescence thermometers. J. Lumin. **236**, 118103 (2021). https://doi.org/10.1016/j.jlumin.2021.118103
19. C.L. Gu, V. Dubey, K.K. Kushwah et al., Thermoluminescence studies of β and γ-irradiated geological materials for environment monitoring. J. Fluoresc. **30**, 819–825 (2020). https://doi.org/10.1007/s10895-020-02536-9
20. S.Y. Zhang, K.Y. Tang, H.J. Fan et al., A competitive radioluminescence material-LiF: Mg, Cu, P for real-time dosimetry. Radiat. Meas. **151**, 106719 (2022). https://doi.org/10.1016/j.radmeas.2022.106719
21. Z.Y. Xiong, Q. Tang, C.X. Zhang, Investigation of thermoluminescence in $Li_2B_4O_7$ phosphors doped with Cu, Ag and Mg. Sci. China Ser. G **50**, 311–320 (2007). https://doi.org/10.1007/s11433-007-0020-3
22. H.Y. Xiao, G. Duan, X.T. Zu et al., Ab initio molecular dynamics simulation of pressure-induced phase transformation in BeO. J. Mater. Sci. **46**, 6408–6415 (2011). https://doi.org/10.1007/s10853-011-5590-9
23. Y. Wang, N. Can, P.D. Townsend, Influence of Li dopants on thermoluminescence spectra of $CaSO_4$ doped with Dy or Tm. J. Lumin. **131**(9), 1864–1868 (2011). https://doi.org/10.1016/j.jlumin.2011.04.042
24. M. Pietriková, J. Krása, L. Juha, Thermoluminescence glow curves of CaF_2: Dy crystals irradiated by soft X-rays. Z. Phys. B Condensed Matter. **93**, 63–66 (1993). https://doi.org/10.1007/BF01308808
25. Y.W. Wei, Y.J. Dong, T. Zhang et al., Influence of reaction of Al_2O_3 and carbonaceous materials in Al_2O_3-C refractories on aluminum and carbon pick-up of iron. J. Iron Steel Res. Int. **27**, 55–61 (2020). https://doi.org/10.1007/s42243-019-00352-5
26. W.J. Ma, Q. Tang, C.X. Zhang et al., Thermoluminescent spectra of MgB_4O_7doped with Mn and Dy. Nucl. Tech. **33**(01), 31–34 (2010). (**in Chinese**)
27. K.H. Gavhane, M.S. Bhadane, P.P. Kulkarni, Investigation of novel Eu doped $SrDy_2O_4$ microphosphor for thermoluminescence dosimetry. J. Lumin. **231**, 117781 (2021). https://doi.org/10.1016/j.jlumin.2020.117781
28. K.H. Gavhane, M.S. Bhadane, P.P. Kulkarni et al., Investigation of novel Eu doped $SrDy_2O_4$ microphosphor for thermoluminescence dosimetry. J. Lumin. **231**, 117781 (2021). https://doi.org/10.1016/j.jlumin.2020.117781
29. Y. Alajlani, N. Can, Thermoluminescence glow curve analysis and kinetic parameters of Dy-doped $BaSi_2O_5$ phosphor. J. Rare Earths **40**, 234–242 (2022). https://doi.org/10.1016/j.jre.2020.10.020
30. I.C. Chen, T.M. Chen, Sol–gel synthesis and the effect of boron addition on the phosphorescent properties of $SrAl_2O_4$:Eu^{2+}, Dy^{3+} phosphors. J. Mater. **16**, 644–651 (2001). https://doi.org/10.1557/JMR.2001.0122
31. V. Chernov, P. Salas-Castillo, L.A. Díaz-Torres, Thermoluminescence and infrared stimulated luminescence in long persistent monoclinic $SrAl_2O_4$:Eu^{2+}, Dy^{3+} and $SrAl_2O_4$:Eu^{2+}, Nd^{3+} phosphors. Opt. Mater. **92**, 46–52 (2019). https://doi.org/10.1016/j.optmat.2019.04.015
32. S. Som, M. Chowdhury, S.K. Sharma, Kinetic parameters of γ-irradiated Y_2O_3 phosphors: effect of doping/codoping and heating rate. Radiat. Phys. Chem. **110**, 51–58 (2015). https://doi.org/10.1016/j.radphyschem.2015.01.015
33. B. Zhao, S.L. Hu, D. Wang, Inhibitory effect of gamma irradiation on Penicillium digitatum and its application in the preservation of Ponkan fruit. Sci. Hortic. **272**, 109598 (2020). https://doi.org/10.1016/j.scienta.2020.109598
34. F.M. Li, Y.B. Gu, D.H. Chen, Study on radiation preservation of frozen egg liquid. Radiat. Phys. Chem. **57**, 341–343 (2000). https://doi.org/10.1016/S0969-806X(99)00401-6
35. R.D.J. Shannon, Revised effective ionic radii and systematic study of inter atomic distances in halides and chalcogenides. Acta. Crystallogr. A. **32**(SEP1), 751–767 (1976). https://doi.org/10.1107/S0567739476001551
36. S. Zhang, H. Yang, H. Yang et al., Vibrational spectroscopic and crystal chemical analyses of double perovskite Y2MgTiO6 microwave dielectric ceramics. J. Am. Ceram. **103**, 16737 (2019). https://doi.org/10.1111/jace.16737
37. H. Liu, J.Y. Guo, X.Y. Li et al., Luminescence and temperature sensing properties of $Y_{2-x-y}Tm_xSm_yMgTiO_6$ phosphors. J. Lumin. **267**, 120392 (2024). https://doi.org/10.1016/j.jlumin.2023.120392
38. Z.T. Fan, S.L. Bi, J. Wang et al., Photoluminescence properties and energy transfer of double perovskite Ca_2LaTaO_6:Bi^{3+}, Tb^{3+} phosphor. J. Lumin. **252**, 119396 (2022). https://doi.org/10.1016/j.jlumin.2022.119396
39. K. Li, D. Mara, R. Van Deun, Synthesis and luminescence properties of a novel dazzling red-emitting phosphor $NaSr_3SbO_6$:Mn^{4+} for UV/n-UV w-LEDs. Dalton Trans. **48**, 3187–3192 (2019). https://doi.org/10.1039/C8DT04827D
40. H. Liu, J.Y. Guo, J.Y. Xu et al., Luminescence properties and energy-transfer behavior of $Y_{2-x-y}Bi_xEu_yMgTiO_6$ phosphors. Heliyon **9**(8), e19063 (2023). https://doi.org/10.1016/j.heliyon.2023.e19063
41. T. Srikanth, D.V. Krishna Reddy, K.S. Rudramamba et al., Red light component tuning by n-UV/blue light excitations in Sm^{3+} /Eu^{3+} co-doped Y_2O_3-Al_2O_3-Bi_2O_3-B_2O_3-SiO_2 glasses for W-LED applications. Opt. Mater. **134**, 113148 (2022). https://doi.org/10.1016/j.optmat.2022.113148
42. N.S. Huang, K. Li, H.X. Deng, BRIGHT: the three-dimensional X-ray crystal Bragg diffraction code. Nucl. Sci. Tech. **30**, 39 (2019). https://doi.org/10.1007/s41365-019-0559-5
43. R.S. Yadav, Energy transfer induced color tunable photoluminescence in Tb^{3+}/Sm^{3+} co-doped Y_2O_3 nano-phosphor for warm white LEDs. J. Alloys Compd. **931**, 167579 (2023). https://doi.org/10.1016/j.jallcom.2022.167579
44. H. Liu, Z.Y. Xiong, C.X. Zeng et al., Luminescence characteristics of $Y_{2-x-y}Bi_xEu_yMgTiO_6$ phosphors. Nucl. Tech. (in Chinese) **46**, 060501 (2023). https://doi.org/10.11889/j.0253-3219.2023.hjs.46.060501
45. Z.Y. Xiong, X.C. Wang, Y.T. Liang, et al., Study of thermoluminescence, photoluminescence and dosimetry for the YAGG:Ce($Y_{2.96}Al_{3.4}Ga_{1.6}O_{12}$:0.04Ce) phosphor. Appl. Radiat. Isot. **193**, 110615 (2023). https://doi.org/10.1016/j.apradiso.2022.110615
46. J.Y. Guo, M. Gao, Z.Y. Xiong et al., Thermoluminescence of natural quartz grains beside Huguangyan Maar Lake. J. Phys. Conf. Ser. **2470**, 012004 (2023). https://doi.org/10.1088/1742-6596/2470/1/012004
47. M.L. Zhan, Y.Y. Chen, Z. Xu, et al., Investigation on thermoluminescence of phosphor YGaAG:Ce($Y_{2.96}Ce_{0.04}Al_{3.4}Ga_{1.6}O_{12}$). Nucl. Tech. (in Chinese) **43**, 050501 (2020). https://doi.org/10.11889/j.0253-3219.2020.hjs.43.050501